Yielding in an Integer Automaton Model for Amorphous Solids under Cyclic Shear

Kareem Khirallah, Botond Tyukodi, Damien Vandembroucq, and Craig E. Maloney

Phys. Rev. Lett. **126**, 218005 — Published 28 May 2021

DOI: 10.1103/PhysRevLett.126.218005

Yielding in an integer automaton model for amorphous solids under cyclic shear

Kareem Khirallah[1],Botond Tyukodi[1,2], Damien Vandembroucq[3],Craig E. Maloney[1]
(1) Northeastern University, Boston, MA, 02115, USA
(2) Department of Physics, Brandeis University, Waltham, MA 02454, USA. and
(3) PMMH, CNRS, ESPCI Paris, Université PSL,
Sorbonne Université, Université de Paris, F-75005 Paris, France

We present results on an automaton model of an amorphous solid under cyclic shear. After a transient, the steady state falls into one of three cases in order of increasing strain amplitude: i) pure elastic behavior with no plastic activity, ii) limit cycles where the state recurs after an integer period of strain cycles, and iii) irreversible plasticity with long-time diffusion. The number of cycles, N required for the system to reach a periodic orbit diverges as the amplitude approaches the yielding transition between regimes ii) and iii) from below, while the effective diffusivity, D of the plastic strain field vanishes on approach from above. Both of these divergences can be described by a power-law. We further show that the average period, T, of the limit cycles increases on approach to yielding.

The behavior of many athermal amorphous solids – emulsions, foams, non-Brownian suspensions of soft particles, compressed granular materials – exhibits a common phenomenology. At small stresses and strains, elasticity prevails, loading is essentially reversible, and the material comes back to its original shape when unloaded without any dissipation of energy. At larger stresses and strains, however, the situation is more subtle. There are many different ways to characterize yielding in these materials. One could ask at what point the material begins to: i) exhibit dissipative events where the energy input by the external drive begins to become dissipated; ii) become mechanically irreversible in the sense of retaining a residual strain when unloaded to zero stress; or iii) become microscopically irreversible in the sense that the system does not return to its original microscopic configuration when unloaded. Recent work has shown, perhaps surprisingly, that these different notions of yielding can be subtly distinct.

Lundberg *et. al.* [1] studied experiments and computer simulations of two dimensional (2D) bubble rafts. They found that, under cyclic shear at strains of around 40%, reversible and irreversible energy-dissipating events could coexist. In the reversible transitions, a local configuration of particles would undergo a topology change during forward shear but revert to its original topology upon reversal, while the irreversible transformations would never revert. Keim and Arratia [2, 3] studied a raft of a polystyrene particles at an oil-water interface driven in a planar Couette shear flow and observed similar reversible and irreversible topological transformations. At the smallest strain amplitude, all transformation eventually went away after many cycles. Then at larger strain amplitude, irreversible transformations eventually went away after many cycles, while reversible transformations remained. Finally at the largest strain amplitudes irreversible transformations persisted indefinitely. Knowlton *et. al.* [4] studied a disordered emulsion at various droplet volume fraction. They used a digital image correlation technique to analyze confocal microcopy images to infer droplet displacements during each full cycle and found a sharp transition as a function of strain amplitude in the single-cycle mean squared displacement, similar in spirit to Keim's measurements of the topological transformations, and used this to define a yielding threshold.

Progress has also been made in particle-based computer simulations. Priezjev [5] performed low temperature molecular dynamics (MD) simulations of a Lennard-Jones (LJ) glass and also observed a transition from reversible transformations at small strain to irreversible at larger strain. Fiocco *et. al.* [6] performed athermal quasistatic (AQS) simulations of a similar LJ glass and similarly found a sharp transition from reversible to irreversible transformations at a characteristic strain with a growing diffusion coefficient in the irreversible regime. Regev *et. al.* [7] also performed AQS simulations of a LJ glass. Their observations were a bit more nuanced. They found that below a critical strain amplitude, after many cycles, the system eventually settled into a so-called n-cycle where it would return to its initial configuration after not 1, but, rather n strain cycles. The characteristic number of strain cycles required to reach this limiting periodic orbit was shown to diverge as the strain amplitude approached the yield strain, but, importantly, their periods remained unstudied. More recently Kawasaki and Berthier [8] have performed MD-like simulations and have analyzed both *single-cycle* stroboscopic information as in Knowlton *et. al.* [4] and also looked at long-time diffusion as in references [5] and [6] where they found a first-order like discontinuous jump in both these quantities at the yielding point. Other theoretical works have also appeared recently addressing the issue of reversibility in cyclic shear [9–12].

Here we study a meso-scale, integer automaton model for amorphous plasticity in the AQS limit. The model is similar to many others proposed recently (see [13] for a review), but it is unique in that it is deterministic after the system is initialized (see also Refs [14, 15] in

a close spirit for crystalline plasticity). This makes it appropriate to map onto experiments and deterministic particle-based simulations of athermal systems. We show that despite its dramatic simplicity compared to particle-based models, it captures their essential emergent behavior, and importantly, the existence of the non-trivial limit cycles during which reversible plastic relaxation occurs. Furthermore, owing to the reduced computational complexity, we are able to gain detailed information about the statistics of the periods of the limit cycles and how they vary on approach to the yielding transition. Finally, we show that the average period grows on approach to yielding.

Our 2D mesoscale model is based on shear transformations [13]. Details are specified in the SI, but briefly: the plane is tiled into discrete elements. The total strain, ϵ_t, at each site is additively decomposed into an elastic and plastic piece: $\epsilon_t = \epsilon_e + \epsilon_p$. ϵ_e gives rise to stress, $\sigma = \mu\epsilon_e$, and we set $\mu = 1$, so ϵ_e and σ are completely interchangeable. The plastic thresholds are set to $+1$ and -1 in the forward and backward directions, respectively. The plastic strain increment $\delta\epsilon_p$ is set to 2, which guarantees a single-valued strain energy function as explained in the SI. During a local yielding event, ϵ_p is updated at the locus of yielding and only there, while ϵ_t and ϵ_e are updated by equal amounts everywhere else according to the rules of linear elasticity in analogy with Eshelby's classical solution for a plastic inclusion in an elastic matrix (see the SI and reference [13] for details).

Many previous works have employed similar models [16–32], but the model we use here is different in a few crucial ways. In particular, we use an integer valued ϵ_p field with no stochasticity aside from the random initial conditions we impose on the ϵ_p field. Precise details are spelled out in the Supplementary Material along with references to related models [13, 17, 20, 22, 23, 30, 32–38]. [39] The dynamical evolution rules for the automaton are: i) for a given stress field, synchronously allow all sites over threshold to yield and recompute the stress field everywhere, ii) repeat this until all sites are below threshold, iii) advance the globally applied total strain until precisely one site is at its stability threshold. Implementing the model as a deterministic automaton allowed us to obtain the periodic limit cycles we describe below analogous to those observed in particle-based simulations [7]. In this study, we used a 128x128 tiling and an ensemble of 20 systems. The system was initialized from a uniform stress free state by imposing a random uncorrelated plastic strain field and then allowing the system to relax. This procedure corresponds to a rapid quench from a high temperature state. The σ (and ϵ_p) field in this quenched state has spatial correlations similar to particle-based simulations [36–38].

After initialization, the system was subjected to cyclic shear at various strain amplitudes, γ_0. In figure 1a), we show the plastic strain for one typical member of the ensemble as a function of the total accumulated strain for three typical strain amplitudes, $\gamma_0 = 0.35, 0.40, 0.55$ representative of the perfect elastic, reversible plastic, and irreversible diffusive regimes respectively. Movies of typical systems are provided in the supplementary material. At early times, plasticity is observed for all three amplitudes. At later times, the three curves behave qualitatively differently. After the seventh strain cycle, the $\gamma_0 = 0.35$ system reaches a fixed value of the plastic strain after which all plastic activity ceases; this is the perfect elastic regime. After eight cycles, the $\gamma_0 = 0.40$ system locks into a period-1 limit cycle where the system has plastic activity, but returns to an identical configuration every full cycle. This is the reversible plastic regime. We will show evidence below for more complicated cases with period greater than 1. Finally the $\gamma_0 = 0.55$ curve experiences a random amount of plastic strain increase/decrease during the forward/backward strain sweeps and never locks into a limit cycle. The system never visits a previous configuration. This is the irreversible diffusive regime.

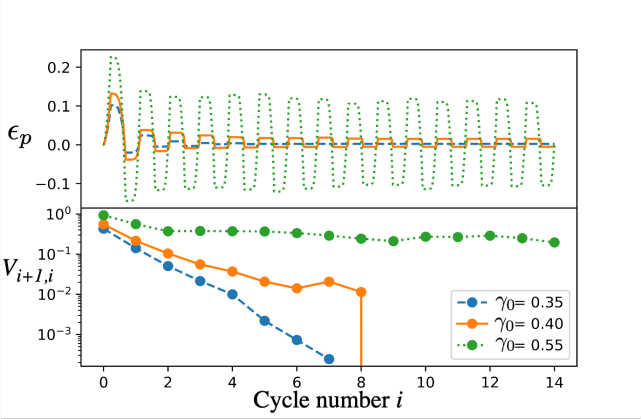

FIG. 1. a) Total plastic strain ϵ_p , and b) the mean squared value,$V_{i+1,i}$, of the single-cycle-incremental plastic strain for a particular realization. Both are plotted vs cycle number for three cycling amplitudes, γ_0: 0.35, 0.4, and 0.55.

To measure decorrelation, we define $V_{i,j}$ to be the ensemble-averaged variance of the incremental plastic strain field defined between cycle i and j: $V_{i,j} = \langle(\epsilon_p(x,y;j) - \epsilon_p(x,y;i))^2\rangle_{x,y}$ where $\epsilon_p(x,y;i)$ is the plastic strain field at cycle i at site (x,y). In figure 1b), we show $V_{i,i+1}$ corresponding to the decorrelation in a single cycle for the same three systems as in figure 1a). For $\gamma_0 = 0.35$, $V_{i,i+1}$ vanishes at $i = 7$ indicating that the consecutive ϵ_p fields become identical after 7 cycles. For $\gamma_0 = 0.40$, $V_{i,i+1}$ vanishes at $i = 8$ indicating that the consecutive microscopic configurations become identical after 8 cycles. For $\gamma_0 = 0.55$, $V_{i,i+1}$ never vanishes and recedes to a plateau, indicating the single-cycle decorrelation of ϵ_p. One might be tempted to relate this single-cycle decorre-

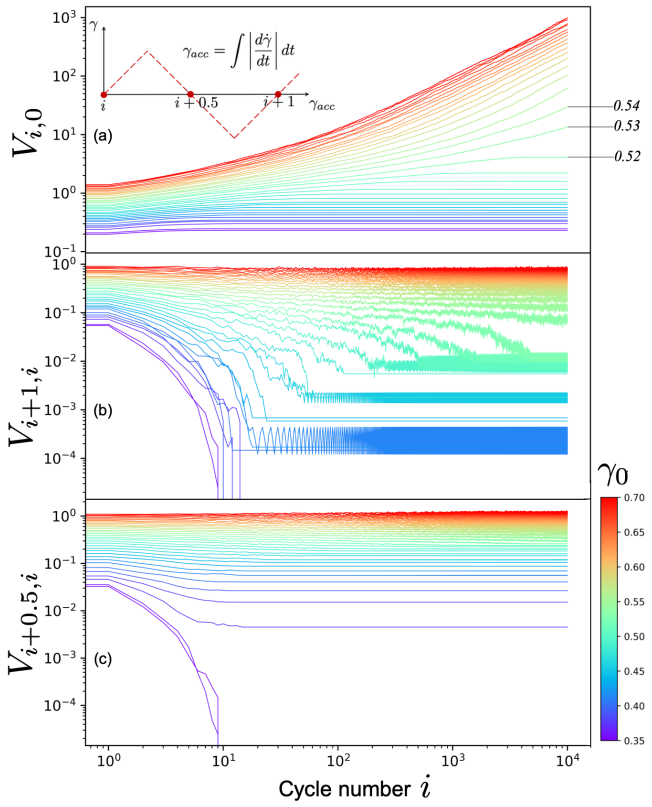

FIG. 2. a) Ensemble average of the decorrelation with respect to the initial configuration $V_{i,0}$ vs cycle number i for different maximum strain amplitude from lowest (bottom) to highest (top) in the range from 0.35 to 0.7 with an increment of 0.01. (Inset) schematic representation of the cycling protocol where $\gamma(t)$ is the current applied strain (which can be positive or negative), γ_0 is the cycling amplitude, and $\gamma_{\rm acc} = \int_0^t |\frac{d\gamma}{dt}| dt$ is the total accumulated strain. b) Ensemble average of the single-cycle decorrelation $V_{i,i+1}$ for the same set of cycling amplitudes as in a). c) Ensemble average of the single-half-cycle (for forward going half-cycles) decorrelation $V_{i,i+1/2}$ for the same set of cycling amplitudes as in a).

lation to the diffusivity of the system as in reference [4], however, as we show below, these two quantities are not simply related.

Figure 2a) shows $V_{i,0}$, the decorrelation with respect to the initial configuration, versus the cycle number for various amplitudes. These curves qualitatively resemble creep-compliance curves in glassy materials [40–44]. All systems, regardless of cycling amplitude, show at least some initial decorrelation as initial plastic activity takes the configuration away from the virgin quenched configuration. However, the systems at the lowest cycling amplitude quickly cease all plastic activity after a few cycles; a perfectly elastic regime is reached, and $V_{i,0}$ saturates at a constant value as the ϵ_p field becomes constant in time. The reversible plastic systems at intermediate amplitude show a period of rise before entering a limit cycle. Once in the limit cycle, the $V_{i,0}$ value will oscillate among a small set of values corresponding to the decorrelation of each of the configurations in the limit cycle with respect to the initial quenched state, but these small variations are not visible on the scale of the figure. For the strain amplitudes above the transition in the irreversible, diffusive regime, the decorrelation continues to grow indefinitely.

Figure 2b) and c) show $V_{i,i+1}$ and $V_{i,i+1/2}$, the full-cycle and half-cycle decorrelation respectively for the same cycling amplitudes as in a). We point out that using single-cycle stroboscopic information alone does *not* allow one to distinguish between period-1 limit cycles and the trivial case with no plasticity, while half-strobe information does allow for this distinction. For instance, for the half-cycle strobe curves in c), we see that only the two ensembles with smallest amplitude reach a trivial state with no plastic activity in any members of the ensemble. When we compare c) to b) we see that 3 more amplitudes show zero full-cycle decorrelation in addition to those two which showed zero decorrelation even for the half-cycle strobe. What this tells us is that those 3 new amplitudes have at least one member of the ensemble which has reached a non-trivial limit cycle with period-1 as opposed to the two smallest amplitudes for which all members of the ensemble reached a trivial limit. For this reason, the transition identified in experiments [4] and simulations [8] via single-full-cycle stroboscopic analysis may not be the yielding transition we identify here where one first sees long-time diffusion, but rather simply the onset of limit cycles with period greater than 1. This transition at the onset of limit cycles would show a discrete jump in the one-cycle stroboscopic de-correlation but would show zero long time diffusion on both sides of the transition. Furthermore, we show, in the supplementary material, how an analysis like that performed in [8], with a limited number of total cycles and a one-time definition of the diffusion constant without checking for stationarity, could lead one to infer a jump in D, while studying a larger number of cycles and checking carefully for stationarity with a two-time definition eliminating the effect of the transient makes the apparent jump go away. We suspect this is one reason there is currently no consensus in the community about whether the yielding transition under cyclic loading is first or second order. At the same time, if one only studies correlation between the current configuration and the initial configuration, e.g., via $V_{i,0}$ [5, 6], one would not be able to differentiate between a pure elastic limit with no plastic dissipation and reversible plastic limit cycles. Rather, one would need to search explicitly for the limit cycles by searching for identical configurations in the past as first pointed out by Regev *et. al.* [7].

To define the number of cycles, N, required to reach a limit cycle (of any period) we compare the terminal configuration in each cycle to the 100 previous ones, so we

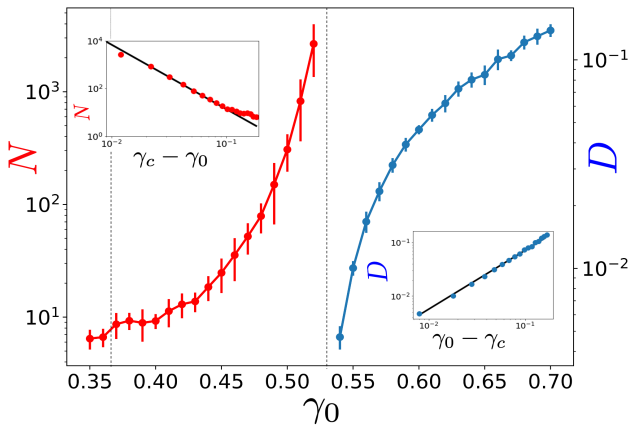

FIG. 3. Left axis: ensemble-averaged number of cycles, N, required to converge to periodic (or trivial) limit cycle. Right axis: diffusion coefficient, D, (defined in the text) for the ϵ_p field. We omit the two points for which the variance of ϵ_p did not reach a diffusive limit on the timescale for which we were able to simulate (10,000 strain cycles). The insets show log-log plots for D and N vs. $|\gamma_0 - \gamma_c|$ where $\gamma_c = 0.532$ against power laws of exponents -2.7 and 1.1, respectively .

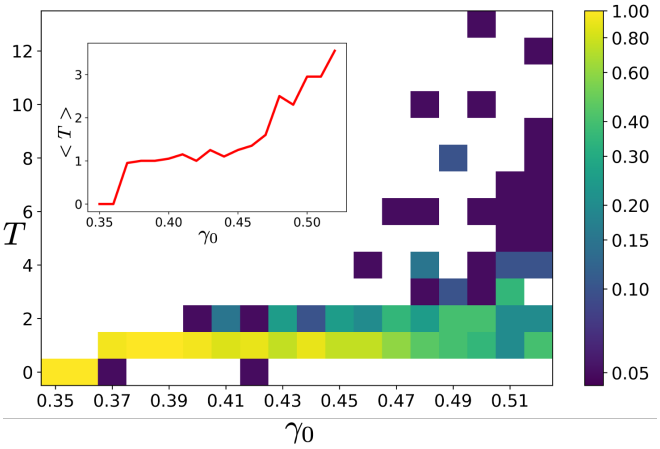

FIG. 4. Probability of the observed periods, T, of terminal limit cycles. Each column represents the probability of observed periods at a particular amplitude for an ensemble of 20 systems. The color scale is logarithmic ranging from 0.05 to 1.0. White indicates no observations, or probability= 0, of a particular period. The inset shows the average period. Pure elastic behavior is treated as $T = 0$.

would not detect cycles with periods greater than 100. In this data set, we have not observed any cycles with periods greater than 13, so it is reasonable to assume that we have not missed any with periods greater than 100. Furthermore, we observe that $V_{0,i}$ is monotonically increasing with i, ruling out high period limit cycles. [45] In figure 3 we show, as a function of cycling amplitude, both (left) the ensemble-averaged number of cycles, N, required to converge to periodic (or trivial) limit cycle for systems below the yielding transition, and (right) a diffusion coefficient, D, for the ϵ_p field for systems above the yielding transition. For amplitudes of 0.52 and below, we find that all the systems in our ensemble have converged to a periodic limit cycle after 10,000 strain cycles, and the average time-to-convergence is well defined. For amplitudes of 0.54 and above, all systems have converged to a diffusive limit, and we can define an effective diffusion coefficient, D, by simply taking: $D = V_{10^4,10^3}/(10^4 - 10^3)\gamma_0$ [46]. We find that, for the strain amplitudes and system sizes studied here, taking data after 10^3 cycles is enough to give statistical stationarity (see SI for details). For $\gamma_0 = 0.53$, we observe that a small number of our systems have converged to a limit cycle but the majority have not. For a finite system size, it is not clear whether it would be possible for an ensemble at one strain amplitude to have co-existence between limit cycles and diffusion, so in principle, it could be possible to define a diffusion coefficient for $\gamma_0 = 0.53$ even if some members of the ensemble have converged to a limit cycle, as long as others continue to diffuse indefinitely. However, in practice we find that $\partial \ln V_{i,10^3}/\partial \ln i$ has not yet reached a constant plateau by $i = 10^4$, so we choose to omit $\gamma_0 = 0.53$ from the plot. In the insets, we show that N and $1/D$ diverge at $\gamma_c = 0.532$ with exponents 2.7 and 1.1 respectively.

In figure 4, we plot histograms of the observed periods of the limit cycles at various cycling amplitudes below the yielding transition. Systems which eventually exhibit perfectly elastic behavior with no plasticity are considered to have period 0. For amplitudes of 0.36 and below, all systems have period zero, *i.e.* all plasticity eventually vanishes. At an amplitude of 0.37, 19 out of 20 systems converge to a period-1 limit cycle while one system eventually reaches a perfect elastic limit. At an amplitude of 0.40, we observe our first limit cycle with period greater than 1. As the amplitude increases toward yielding, the average period increases. In the inset, we plot the ensemble-averaged period vs. cycling amplitude which shows the tendency to increase.

In summary, we have found three regimes (elastic, reversible plastic, diffusive) in our cyclicly sheared automaton model which are consistent with previous experiments [1–3] and particle-based simulations [5–7]. We have found power laws on approach to γ_c for: i) the number of cycles, N, required to reach a limit cycle below γ_c and ii) the effective diffusion constant, D, above γ_c. We also reported the distribution of periods of the limit cycles below γ_c and showed that the average period grew on approach to γ_c. These results were enabled by the high computational efficiency of the automaton allowing us to reach 10^4 cycles which is two orders of magnitude beyond what can currently be obtained in experiment or parti-

cle simulation. We hope our results will stimulate future work on experiments and particle-based simulations to address the issue of the periods of the limit cycles and the power-law form of D and N.

There are many open questions and routes for future work. i) A more detailed study of the critical region should be performed with a finer sweep of strain amplitudes along with a finite size scaling analysis of N and D along with larger ensembles to understand the distribution of limit-cycle periods. ii) The effective diffusion coefficient studied here is for the diffusion of the plastic strain rather than the diffusion of the displacement as is conventionally studied in experiments and particle-based simulations. Some of us have already shown that there is a non-trivial relationship between strain-based statistics and displacement-based statistics in steady shear [47–49], and one would expect a similar non-trivial relationship here in the cyclic case. iii) We have observed that *even in the yielded-diffusive regime* a significant fraction of the plasticity in a forward sweep reverses itself during the subsequent backward sweep; this is remarkable and deserves further study. iv) The issue of sample preparation recently raised in Ref. [50, 51] is, perhaps, most important of all, as it is well known that sample age/preparation/quench protocol is crucial even in steady shear [52–57] , and therefore it will be important to study systems which have been prepared with a gentler quench or annealed or subjected to small (subyield) cyclic strain before the main cycling. It is only through these more complex protocols that we will discover how the material encodes memory of its history via its state[51, 58, 59].

Acknowledgement This research was supported in part by the National Science Foundation under Grant No. NSF PHY-1748958 and CMMI-1822020.

[1] Micah Lundberg, Kapilanjan Krishan, Ning Xu, Corey S O'Hern, and Michael Dennin. Reversible plastic events in amorphous materials. *Phys. Rev. E*, 77(4):041505, 2008.

[2] Nathan C Keim and Paulo E Arratia. Mechanical and microscopic properties of the reversible plastic regime in a 2d jammed material. *Phys. Rev. Lett.*, 112(2):028302, 2014.

[3] Nathan C Keim and Paulo E Arratia. Yielding and microstructure in a 2d jammed material under shear deformation. *Soft Matter*, 9(27):6222–6225, 2013.

[4] Elizabeth D Knowlton, David J Pine, and Luca Cipelletti. A microscopic view of the yielding transition in concentrated emulsions. *Soft Matter*, 10(36):6931–6940, 2014.

[5] Nikolai V Priezjev. Heterogeneous relaxation dynamics in amorphous materials under cyclic loading. *Phys. Rev. E*, 87(5):052302, 2013.

[6] Davide Fiocco, Giuseppe Foffi, and Srikanth Sastry. Oscillatory athermal quasistatic deformation of a model glass. *Phys. Rev. E*, 88(2):020301, 2013.

[7] Ido Regev, Turab Lookman, and Charles Reichhardt. Onset of irreversibility and chaos in amorphous solids under periodic shear. *Phys. Rev. E*, 88(6):062401, 2013.

[8] Takeshi Kawasaki and Ludovic Berthier. Macroscopic yielding in jammed solids is accompanied by a nonequilibrium first-order transition in particle trajectories. *Physical Review E*, 94(2):022615, 2016.

[9] Srikanth Sastry. Models for the yielding behaviour of amorphous solids, 2020.

[10] Chen Liu, Ezequiel E. Ferrero, Eduardo A. Jagla, Kirsten Martens, Alberto Rosso, and Laurent Talon. Oscillatory quasistatic shear deformation of amorphous materials: a mesoscopic approach, 2021.

[11] Ido Regev, Ido Attia, Karin Dahmen, Srikanth Sastry, and Muhittin Mungan. The topology of the energy landscape of sheared amorphous solids and the irreversibility transition, 2021.

[12] Nathan C. Keim and Joseph D. Paulsen. Multiperiodic orbits from interacting soft spots in cyclically-sheared amorphous solids, 2021.

[13] Alexandre Nicolas, Ezequiel E Ferrero, Kirsten Martens, and Jean-Louis Barrat. Deformation and flow of amorphous solids: Insights from elastoplastic models. *Rev. Mod. Phys.*, 90(4):045006, 2018.

[14] O. U. Salman and L. Truskinovsky. Minimal integer automaton behind crystal plasticity. *Phys. Rev. Lett.*, 106:175503, 2011.

[15] R. Baggio, E. Arbib, P. Biscari, S. Conti, L. Truskinovsky, G. Zanzotto, and O. U. Salman. Landau-type theory of planar crystal plasticity. *Phys. Rev. Lett.*, 123:205501, 2019.

[16] J.-C. Baret, D. Vandembroucq, and S. Roux. An extremal model of amorphous plasticity. *Phys. Rev. Lett.*, 89:195506, 2002.

[17] E. A. Jagla. Strain localization driven by structural relaxation in sheared amorphous solids. *Phys. Rev. E*, 76:046119, 2007.

[18] K. A. Dahmen, Y. Ben-Zion, and J. T. Uhl. Micromechanical model for deformation in solids with universal predictions for stress-strain curves and slip avalanches. *Phys. Rev. Lett.*, 102:175501, 2009.

[19] E. R. Homer and C. A. Schuh. Mesoscale modeling of amorphous metals by shear transformation zone dynamics. *Acta Mat.*, 57:2823–2833, 2009.

[20] K. Martens, L. Bocquet, and J.-L. Barrat. Connecting diffusion and dynamical heterogeneities in actively deformed amorphous systems. *Phys. Rev. Lett.*, 106:156001, 2011.

[21] K. Martens, L. Bocquet, and J.-L. Barrat. Spontaneous formation of permanent shear bands in a mesoscopic model of flowing disordered matter. *Soft Matter*, 8:4197, 2012.

[22] M. Talamali, V. Petäjä, D. Vandembroucq, and S. Roux. Strain localization and anisotropic correlations in a mesoscopic model of amorphous plasticity. *C.R. Mécanique*, 340:275–288, 2012.

[23] Z. Budrikis and S. Zapperi. Avalanche localization and crossover scaling in amorphous plasticity. *Phys. Rev. E*, 88:062403, 2013.

[24] A. Nicolas, K. Martens, L. Bocquet, and J.-L. Barrat. Universal and non-universal features in coarse-grained models of flow in disordered solids. *Soft Matter*, 10:4648–4651, 2014.

[25] Jin Lin, E. Lerner, A. Rosso, and M. Wyart. Scaling description of the yielding transition in soft amorphous solids at zero temperature. *Proc. Nat. Acd. Sci.*, 111:14382–14387, 2014.

[26] B. Tyukodi, S. Patinet, S. Roux, and D. Vandembroucq. From depinning transition to plastic yielding of amorphous media: A soft modes perspective. *Phys. Rev. E*, 93:063005, 2016.

[27] Zoe Budrikis, David Fernandez Castellanos, Stefan Sandfeld, Michael Zaiser, and Stefano Zapperi. Universal features of amorphous plasticity. *Nature Comm.*, 8:15928, 2017.

[28] E. A. Jagla. Critical exponents of the yielding transition of amorphous solids. *Phys. Rev. E*, 98:013002, 2018.

[29] Chen Liu, Ezequiel E. Ferrero, Kirsten Martens, , and Jean-Louis Barrat. Creep dynamics of athermal amorphous materials: a mesoscopic approach. *Soft Matter*, 14:8306, 2018.

[30] Botond Tyukodi, Damien Vandembroucq, and Craig E. Maloney. Diffusion in mesoscopic lattice models of amorphous plasticity. *Phys. Rev. Lett.*, 121:145501, 2018.

[31] E. E. Ferrero and E. A. Jagla. Criticality in elastoplastic models of amorphous solids with stress-dependent yielding rates. *Soft Matter*, 15:9041, 2019.

[32] Botond Tyukodi, Damien Vandembroucq, and Craig E. Maloney. Avalanches, thresholds, and diffusion in mesoscale amorphous plasticity. *Phys. Rev. E*, 100:043003, 2019.

[33] Guillemette Picard, Armand Ajdari, François Lequeux, and Lydéric Bocquet. Elastic consequences of a single plastic event: A step towards the microscopic modeling of the flow of yield stress fluids. *The European Physical Journal E*, 15(4):371–381, 2004.

[34] A Onuki. Plastic flow in two-dimensional solids. *Phys. Rev. E*, 68(6, 1), DEC 2003.

[35] M. Talamali, V. Petäjä, D. Vandembroucq, and S. Roux. Avalanches, precursors and finite size fluctuations in a mesoscopic model of amorphous plasticity. *Phys. Rev. E*, 84:016115, 2011.

[36] Yegang Wu, Kamran Karimi, Craig E Maloney, and S Teitel. Anomalous stress fluctuations in athermal two-dimensional amorphous solids. *Phys. Rev. E*, 96(3):032902, 2017.

[37] Anael Lemaitre. Tensorial analysis of Eshelby stresses in 3D supercooled liquids. *J. Chem. Phys.*, 143(16), OCT 28 2015.

[38] Sadrul Chowdhury, Sneha Abraham, Toby Hudson, and Peter Harrowell. Long range stress correlations in the inherent structures of liquids at rest. *J. Chem. Phys.*, 144(12), MAR 28 2016.

[39] A technical detail explained in the Supplementary Material is that for the model to be derivable from a local piecewise continuous strain energy function [34, 60], we must choose the incremental plastic strain associated with a local yielding event to be twice the yield stress. In this letter, we arbitrarily set the threshold to 1 which then requires that the increment be 2.

[40] P. Ballesta and G. Petekidis. Creep and aging of hard-sphere glasses under constant stress. *PHYSICAL REVIEW E*, 93(4), APR 25 2016.

[41] Pinaki Chaudhuri and Juergen Horbach. Onset of flow in a confined colloidal glass under an imposed shear stress. *Phys. Rev. E*, 88(4), OCT 7 2013.

[42] C. Christopoulou, G. Petekidis, B. Erwin, M. Cloitre, and D. Vlassopoulos. Ageing and yield behaviour in model soft colloidal glasses. *PHILOSOPHICAL TRANSACTIONS OF THE ROYAL SOCIETY A-MATHEMATICAL PHYSICAL AND ENGINEERING SCIENCES*, 367(1909):5051–5071, DEC 28 2009.

[43] ML Falk and JS Langer. Dynamics of viscoplastic deformation in amorphous solids. *PHYSICAL REVIEW E*, 57(6):7192–7205, JUN 1998.

[44] F Spaepen. Homogeneous flow of metallic glasses: A free volume perspective. *SCRIPTA MATERIALIA*, 54(3):363–367, FEB 2006.

[45] One advantage of using an integer automaton is that it is relatively quick to do this comparison of integer fields to check whether the system has returned to a previously visited configuration. Although checking for limit cycles in a particle-based simulation should be essentially the same, because of the continuous degrees of freedom and chaotic dynamics, it is not clear what precision one would need to use to decide if one had returned precisely to a previously encountered configuration that would yield an identical future trajectory.

[46] We note that our D here refers to the diffusivity of the plastic strain field rather than particle displacements measured by other groups [5, 6].

[47] Craig E. Maloney and Mark O. Robbins. Evolution of displacements and strains in sheared amorphous solids. *JOURNAL OF PHYSICS-CONDENSED MATTER*, 20(24), JUN 18 2008. Workshop on Mechanical Behavior of Glassy Materials, Pacific Inst Theoret Phys, Vancouver, CANADA, JUL 21-23, 2007.

[48] Botond Tyukodi, Damien Vandembroucq, and Craig E. Maloney. Avalanches, thresholds, and diffusion in mesoscale amorphous plasticity. *PHYSICAL REVIEW E*, 100(4), OCT 23 2019.

[49] Botond Tyukodi, Damien Vandembroucq, and Craig E. Maloney. Diffusion in Mesoscopic Lattice Models of Amorphous Plasticity. *PHYSICAL REVIEW LETTERS*, 121(14), OCT 1 2018.

[50] Markus Blank-Burian and Andreas Heuer. Shearing small glass-forming systems: A potential energy landscape perspective. *Phys. Rev. E*, 98:033002, 2018.

[51] Eden Schinasi-Lemberg and Ido Regev. Annealing and rejuvenation in a two-dimensional model amorphous solid under oscillatory shear. *Physical Review E*, 101:023603, 2020.

[52] Yuliang Jin, Pierfrancesco Urbani, Francesco Zamponi, and Hajime Yoshino. A stability-reversibility map unifies elasticity, plasticity, yielding, and jamming in hard sphere glasses. *Science Advances*, 4(12), 2018.

[53] J Rottler and MO Robbins. Unified description of aging and rate effects in yield of glassy solids. *PHYSICAL REVIEW LETTERS*, 95(22), NOV 25 2005.

[54] F Varnik, L Bocquet, JL Barrat, and L Berthier. Shear localization in a model glass. *PHYSICAL REVIEW LETTERS*, 90(9), MAR 7 2003.

[55] YF Shi and ML Falk. Strain localization and percolation of stable structure in amorphous solids. *PHYSICAL REVIEW LETTERS*, 95(9), AUG 26 2005.

[56] M. L. Manning, J. S. Langer, and J. M. Carlson. Strain localization in a shear transformation zone model for amorphous solids. *PHYSICAL REVIEW E*, 76(5, 2), NOV 2007.

[57] Marko Popovic, Tom W. J. de Geus, and Matthieu Wyart. Elastoplastic description of sudden failure in

athermal amorphous materials during quasistatic loading. *PHYSICAL REVIEW E*, 98(4), OCT 11 2018.

[58] Daniel J. Lacks and Mark J. Osborne. Energy landscape picture of overaging and rejuvenation in a sheared glass. *Phys. Rev. Lett.*, 93:255501, 2004.

[59] Muhittin Mungan, Srikanth Sastry, Karin Dahmen, and Ido Regev. Networks and hierarchies: How amorphous materials learn to remember. *Physical Review Letters*, 123:178002, 2019.

[60] E. A. Jagla. Strain localization driven by structural relaxation in sheared amorphous solids. *PHYSICAL REVIEW E*, 76(4, 2), OCT 2007.